

Phase diagram of solutions of oppositely charged polyelectrolytes

R. Zhang and B. I. Shklovskii

Theoretical Physics Institute, University of Minnesota, Minneapolis, Minnesota 55455

(Dated: October 31, 2019)

Abstract

We study a solution of long polyanions (PA) with shorter polycations (PC) and focus on the role of Coulomb interaction. A good example is solutions of DNA and PC which are widely studied for gene therapy. In the solution, each PA attracts many PCs to form a complex. When the ratio of total charges of PA and PC in the solution, x , is close to 1, the Coulomb repulsion between complexes is small and complexes condense in a macroscopic drop. When x is far away from 1, the Coulomb repulsion is large and free complexes are stable. As x approaches to 1, PCs disproportionate themselves on complexes by two competing ways. One way is inter-complex disproportionation, in which PCs make some complexes neutral and therefore condensed in a macroscopic drop while other complexes become stronger charged and stay free. The other way is intra-complex disproportionation, in which PCs make one end of a complex neutral and condensed in a droplet while the rest of the complex forms strongly charged tail. Thus each complex becomes a “tadpole”. We get a phase diagram of PA-PC solution in a plane of x and inverse screening radius of the monovalent salt, which includes phases with both kinds of disproportionation.

PACS numbers: 61.25.Hq, 82.35.Rs, 87.14.Gg, 87.15.Nn

I. INTRODUCTION

Condensation in solution of two oppositely charged polyelectrolytes (PE) is an important phenomenon in biology and chemical engineering. One of the most interesting applications is DNA condensation by polycations (PC), which is widely used in gene therapy research. A good example is condensation of DNA with poly-lysine [1]. Complexation of DNA with PCs can invert the charge of bare DNA and help DNA to penetrate negatively charged cell membrane. At the same time, adsorbed PC in complexes or their condensate may protect DNA from digestion by enzymes inside the cell [2]. Tremendous amount of experimental work has been done in this area [1, 2, 3, 4, 5, 6, 7].

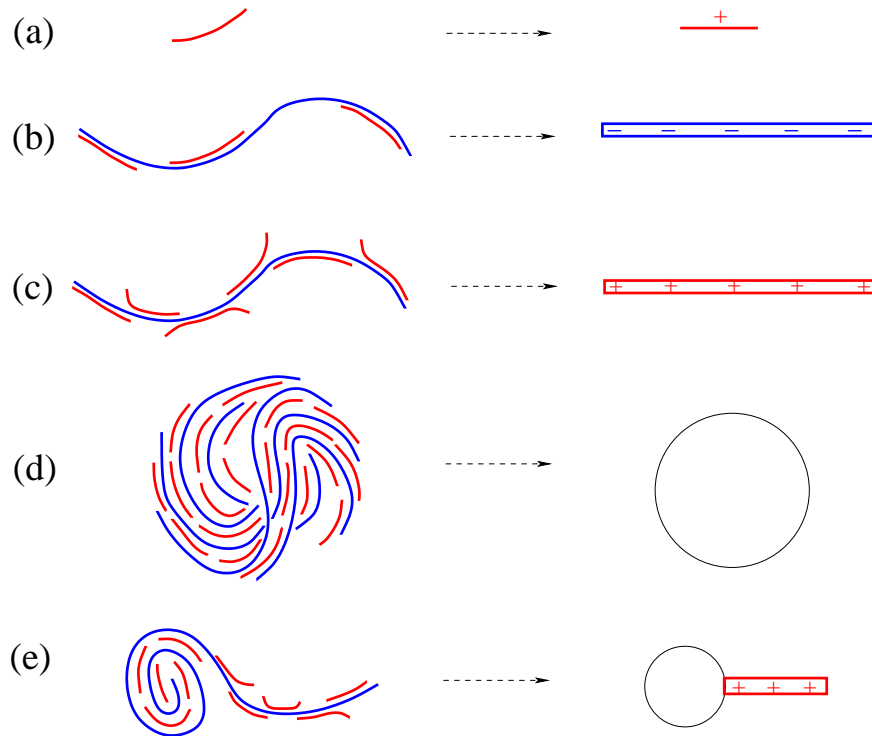


FIG. 1: Objects appearing in a solution of PA and PC (left column) and their symbols used in Figs. 2, 5, 6 and 8 (right column). The long polymer is PA and the short polymer is PC. (a) a single PC. (b) negative PA-PCs complex. (c) positive PA-PCs complex. (d) condensate of almost neutral complexes. (e) tadpole made of one PA-PCs complex. Here only the case of positive tail is shown. The tail can be negative too.

In this paper, motivated by DNA-PC condensation, we study the equilibrium state of a solution of polyanions (PA) and polycations (PC) in the presence of monovalent salt and

focus on the role of Coulomb interaction. We assume that both PA and PC are so long that at room temperature T their translational entropy can be ignored in comparison with the Coulomb energy. We are particularly interested in the case where PA is much longer than PC and many PCs are needed to neutralize one PA. In the solution, each PA attracts many PCs to form a PA-PCs complex (Fig. 1b,c). Neutral complexes can further condense in a liquid drop (Fig. 1d). One complex can form a neutral head and charged tail to become a tadpole (Fig. 1e). And it is possible to have excessive free PCs (Fig. 1a). When and where these objects exist or co-exist with each other depend on two dimensionless parameters: the ratio of total charges of PC and PA in the solution, x , and L/r_s , where L is the length of a free PA-PCs complex and r_s is Debye-Hückel screening radius provided by monovalent salt. The main result of this paper is the phase diagram in a plane of x and L/r_s as shown in Fig. 2. We discover a new phase of “tadpoles” originating from the polymer nature of the objects. We also present a first theory of broadening of the phase of a single drop with decreasing r_s (curves $x_s(r_s)$ and $x'_s(r_s)$ in Fig. 2).

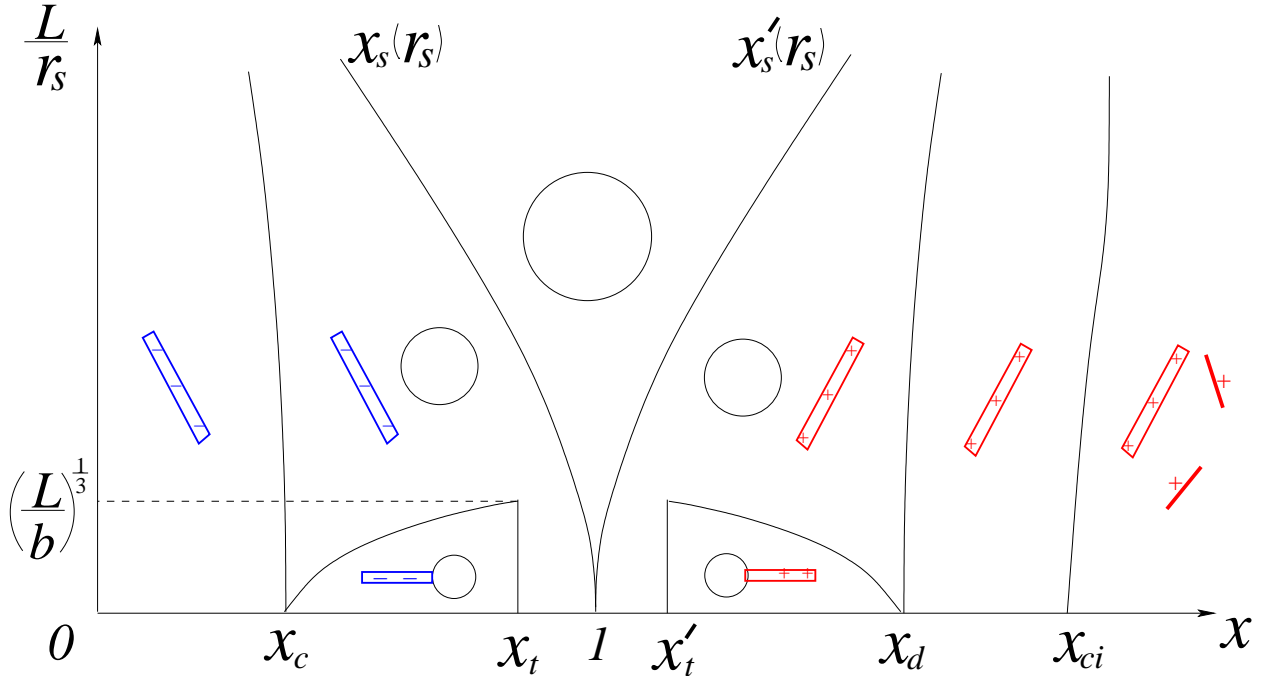


FIG. 2: Typical phase diagram of a solution of PA and PC. The horizontal axis x is the ratio of total charges of PC and PA in the solution. The vertical axis L/r_s is the ratio of the length of a free PA-PCs complex to Debye-Hückel screening radius. Symbols are explained in Fig. 1.

Up to now, there was no theory of phase diagram for such systems. Previously, the complexation of oppositely charged polyelectrolytes was studied in a symmetric system in which the length, concentration and linear charge density of PA and PC are the same [8]. It was shown that even in the absence of monovalent salt, strongly charged PA and PC form a single macroscopic drop of neutral dense liquid which separates from water. It corresponds to the phase at $x = 1$ in our phase diagram (Fig. 2). On the other hand, the phase diagram of a solution of DNA and short polyamines was studied in Refs. [9, 10, 11] in which translational entropy of polyamines plays a very important role. We will discuss the role of this translational entropy only in the very end of this paper (Sec. VI). In our previous works [12, 13], phase diagrams have been discussed for other systems. In Ref. [12], very long PA with positive spheres was considered. This system is similar to chromatin in the sense that each PA binds many spheres making a long necklace. We also discussed the phase diagram of a system of oppositely charged spheres in strongly asymmetric case when each say negative sphere complexes with many positive ones [13]. Many features of the phase diagram in Fig. 2 are also applicable to these systems and we will return to them in the conclusion.

Let us now try to understand the phase diagram of Fig. 2 qualitatively. We start from the horizontal axis ($r_s \rightarrow \infty$). In the solution, each PA adsorbs many PCs to form a complex. When $x < 1$, the number of PC is not enough to neutralize all PAs and each PA-PCs complex is strongly negatively charged (Fig. 1b). When $x > 1$, the number of PC is larger than necessary to neutralize all PAs and each complex is strongly positively charged (charge inverted) (Fig. 1c). In both cases, the Coulomb repulsion between complexes is huge and all complexes stay free, or in other words, colloidal solution of complexes is stable (see ranges $0 < x < x_c$ and $x_d < x < x_{ci}$ in Fig. 2). Let us briefly remind the mechanism of charge inversion at $x > 1$ [14]. We illustrate it in Fig. 3 for the model of strongly charged flexible PA and PC, in which the distance between charges, b , is of the order of Bjerrum length $l_B = 7\text{\AA}$ ($e^2/Dl_B = k_B T$). When a new PC comes to a neutral PA-PCs complex, all PCs in the complex can rearrange themselves so that the charge of this excessive PC is smeared in the whole complex and the Coulomb self-energy of the PC is effectively reduced to zero (Fig. 3). This elimination of the Coulomb self-energy is essentially due to correlation of PCs in the complex and can not be described by Poisson-Boltzmann approximation. We define $\mu_c < 0$ (c stands for ‘‘correlation’’) as the chemical potential related to the elimination of the

Coulomb self-energy of PC in the complex. Related to the charge of PC, it acts as an external voltage overcharging PA. With increasing x , the inverted charge of the complex increases. At certain critical $x = x_{ci}$ (ci stands for “charge inversion”) (see Fig. 2), the maximum charge inversion is achieved where μ_c is balanced by the Coulomb repulsive energy of the complex to a PC.

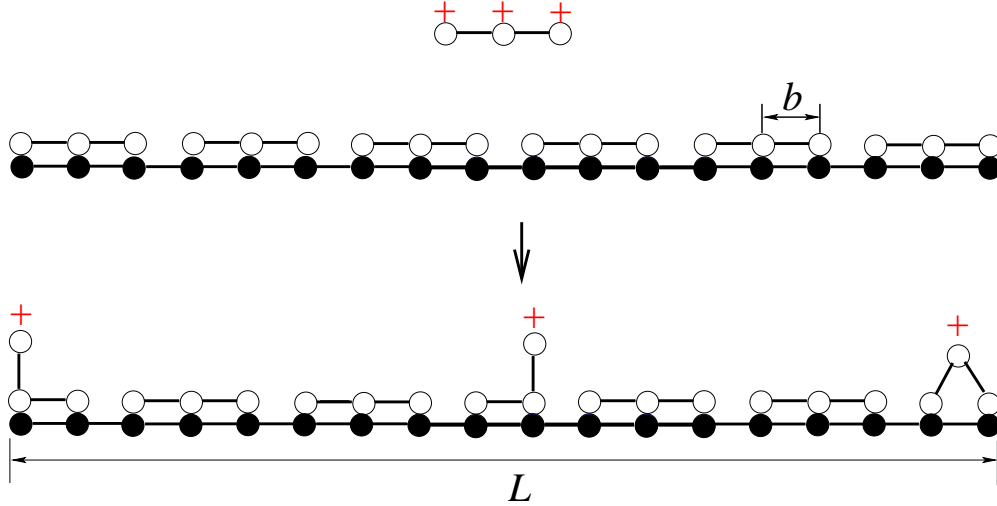


FIG. 3: An illustration of charge inversion of a PA molecule by flexible PCs when they are both strongly charged. Negative PA charges are shown by black dots. Positive PC charges are shown by white dots. When a new PC molecule is adsorbed to a neutral PA-PCs complex, its charge is fractionalized in mono-charges and its Coulomb self-energy is eliminated by redistribution of all PCs in the complex. In reality, the numbers of charges of PA and PC can be much larger than what is shown here.

When $x = 1$, each PA-PCs complex is neutral and there is no Coulomb repulsion between them. They all condense to form a macroscopic strong correlated liquid drop (see Fig. 2). Due to the orderly arrangement of positive and negative charges in the drop, certain amount of short-range correlation energy is gained (Fig. 4). We define $\varepsilon < 0$ as the energy gain of a neutral complex in the macroscopic drop.

In vicinity of $x = 1$, the long-range Coulomb repulsion between charged complexes competes with the short-range attraction due to correlations. To minimize the free energy, PCs can be redistributed among complexes so that a portion of complexes are neutral and therefore condensed in a macroscopic drop, while the rest of complexes become stronger charged

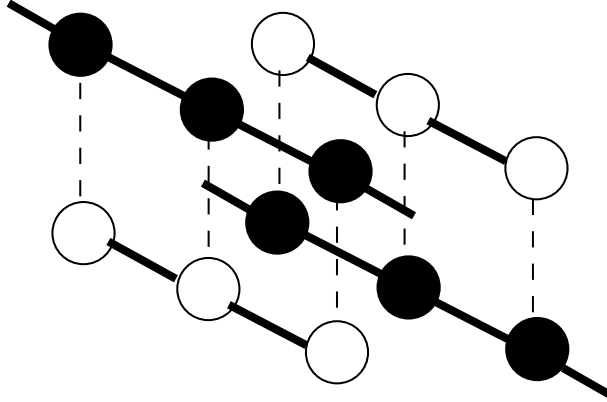


FIG. 4: A schematic illustration of short-range attraction between neutral complexes in a condensed liquid drop using the model of strongly charged PA and PC. A portion of two complexes in the liquid drop is shown. PA and PC charges are shown by black and white dots correspondingly. The dashed lines show two complexes sitting in parallel planes. The complexes attract each other because charges of same sign are farther away than charges of opposite sign.

and stay free. This is called *inter-complex disproportionation* [2] or partial condensation [12] (see Fig. 5a). As $|x - 1|$ grows, the Coulomb energy increases, and the fraction of the condensed complexes becomes smaller. Interestingly, there is a second way to disproportionate. We call it *intra-complex disproportionation* since PCs disproportionate themselves within each complex (Fig. 5b). They move closer to one end of PA molecule, making one part of a PA molecule neutral and condensed in a droplet, while the other part is stronger charged and not condensed. As a result, each complex in the solution forms a “tadpole” with a neutral condensed “head” and a charged “tail” (Fig. 1e). The tail is negative at $x < 1$ and positive at $x > 1$. As $|x - 1|$ grows, the size of the head decreases. At a given x , two ways of disproportionation (Fig. 5) compete with each other. In the tadpole configuration, the Coulomb energy of the system is smaller since the net charge of all PA and PC is shared by all complexes, while the surface energy is larger since there are many droplets. When x is very close to 1, the surface energy dominates and therefore the phase of partial condensation, or inter-complex disproportionation, wins. When x is farther away from 1, the Coulomb energy dominates. Now the tadpole phase, or intra-complex disproportionation, wins. Thus, at $r_s \rightarrow \infty$, we have the sequence of these phases as shown on the horizontal axis of Fig. 2.

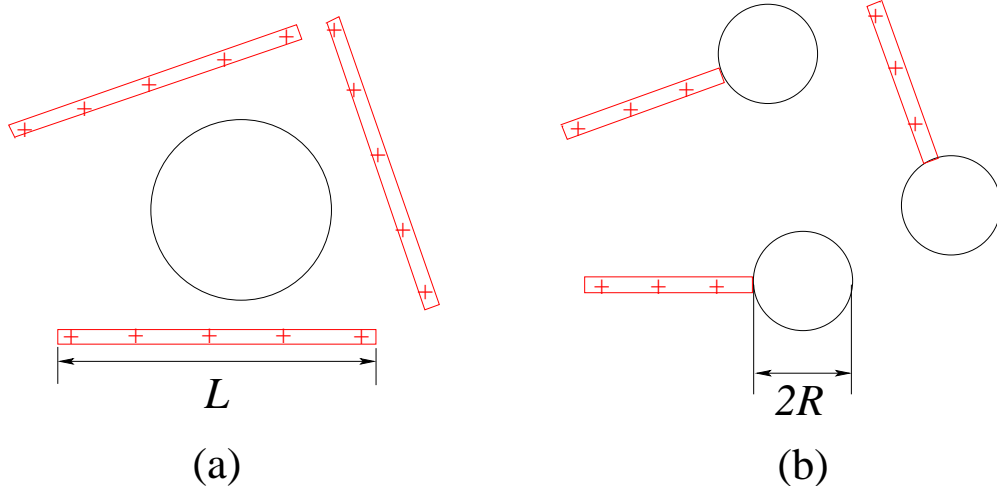


FIG. 5: Two ways to disproportionate. Symbols used here are explained in Fig. 1. (a) inter-complex disproportionation: PCs disproportionate themselves among PAs so that a part of PA-PCs complexes are neutral and condensed in a macroscopic drop, while the rest of them are stronger charged and free. (b) intra-complex disproportionation: PCs disproportionate themselves within each PA-PCs complex to form a “tadpole”, with a neutral condensed “head” and a charged “tail”. Here only the case of positive complexes is showed ($x > 1$). At $x < 1$, all positive charges in tails are replaced by negative ones.

Now let us discuss the effects of screening by a monovalent salt. The screening effectively cuts off the range of the Coulomb interaction at distance r_s . As r_s decreases, first the long-range Coulomb repulsion is reduced while the short-range correlational attraction is not affected. Accordingly, all the ranges of condensation in the phase diagram becomes wider (Fig. 2). Eventually, in the limit of very small r_s , the short-range correlational attraction is also screened out and the macroscopic drop completely dissolves (not shown in Fig. 2). In the intermediate range of r_s we are interested in, there are two major effects of screening. First, the tadpole configuration disappears at certain r_s (Fig. 2). For r_s smaller than this critical value, Coulomb energy is less important and the tadpole phase always loses to the phase of partial condensation. In other words, inter-complex disproportionation wins everywhere in competition with intra-complex disproportionation. Second, the phase of “single drop” (all PAs and PCs are condensed) which for $r_s \rightarrow \infty$ exists only at $x = 1$ at a finite r_s occupies a finite range of x around $x = 1$, which grows with $1/r_s^2$ (Fig. 2). At $r_s \rightarrow \infty$, the macroscopic

drop should be neutral and therefore it exists only at $x = 1$. If each condensed complex were charged ($x \neq 1$), the total charge of the macroscopic drop would be proportional to its volume and Coulomb energy per unit volume would be proportional to its surface which is huge. On the other hand, at r_s much smaller than the size of the macroscopic drop, the Coulomb energy is not accumulative but additive for each volume of size r_s . Therefore the macroscopic drop can tolerate some charge density and the range of the single drop phase in the phase diagram widens.

Currently our theory can be compared with experiments only qualitatively since in many cases it is not clear whether the equilibrium state of the system is reached due to the slow kinetics. In solutions of DNA with PC, charge inversion of complexes is observed at $x > 1$ [1, 2]. The size of condensed particles reaches maximum close to $x = 1$ corresponding to the single drop phase in our phase diagram. When $x \neq 1$, the size of condensed particles decreases which is consistent with our equilibrium phase diagram [1, 2, 3]. In solutions of DNA with basic polypeptides, at $x < 1$, it is observed that DNA molecules exist simultaneously in two distinct conformations, i.e., elongated conformation and condensed conformation [4]. This corresponds to the partial condensation regime in our phase diagram ($x_c < x < 1$ in Fig. 2). On the other hand, the enhancement of condensation with the help of simple salt is observed in Ref. [1]. Certain tadpole-like phases have also been observed in experiments [1, 5, 6].

This paper is organized as follows. In Sec. II, we discuss inter-complex disproportionation. In Sec. III, we study the possibility of intra-complex disproportionation and the tadpole phase. The role of screening by monovalent salt is discussed in Sec. IV. In Sec. V, we estimate parameters ε and μ_c microscopically in the case of strongly charged PA and PC. In Sec. VI, we discuss the role of translational entropy of PC in connection with previous works [12, 13]. We conclude in Sec. VII.

II. INTER-COMPLEX DISPROPORTIONATION

In this section we discuss the basic scheme of PE condensation: inter-complex disproportionation (Fig. 5a). Here and below, We focus on the role of Coulomb interaction and neglect all other interactions such as hydrophobic force. We consider the case where $r_s \rightarrow \infty$ and discuss the role of finite r_s in Sec. IV. We also postpone the discussion of intra-complex disproportionation to Sec. III and the discussion of the translational entropy of PC to Sec. VI.

At x close to 1, inter-complex disproportionation leads to a phase of partial condensation which has the lowest free energy. In this phase, PCs disproportionate themselves among PAs to make a portion of PA-PCs complexes neutral and condensed in a macroscopic drop, while all other complexes are stronger charged and free (Fig. 5a). The Coulomb energy of each charged complex can be calculated by considering it as a metallic object with certain capacitance. Indeed, PCs are free to move along PA and the electric potential is therefore equal along each complex.

Let us define y as the fraction of free complexes and N as the total number of PAs in the solution. The free energy of the system in the condensation regime is

$$F(y) = yN \left[\frac{(nq - Q)^2}{2C} + nE(n) \right] + (1 - y)N[n_i E(n_i) + \varepsilon] \quad (1)$$

Here C is the capacitance of a free complex, $-Q$ and q are the bare charge of PA and PC, n is the number of PC in each free PA-PCs complex, $n_i = Q/q$ is the number of PC in a neutral complex, and $E(n) < 0$ is the correlation energy of a PC in a complex as a function of n . In this expression, the first term is the free energy of free complexes, including the Coulomb self-energy of free complexes and the negative correlation energy of PCs in free complexes. The second term is the free energy of neutral condensed complexes, including the negative correlation energy of PCs in neutral complexes and the negative correlation energy of neutral complexes due to condensation. We emphasize again that we study very long and strongly charged PC and PA such that their translational entropies are negligible.

If we assume all PCs are adsorbed to PAs, the net charge of each free complex, $(nq - Q)$, is equal to $(x - 1)Q/y$, we have

$$n = \frac{(x + y - 1)Q}{yq}. \quad (2)$$

We will show in Sec. V that in the condensation regime, $|n - n_i| \ll n_i$. Consequently, $\mu_c(n) = \partial[nE(n)]/\partial n$ is approximately equal to its value μ_c at $n = n_i$. Using Eq. (2) and the definition of μ_c , we rewrite the free energy as

$$F(y) = yN \frac{(x - 1)^2 Q^2 / y^2}{2C} + yN \frac{(x - 1)Q/y}{q} \mu_c + (1 - y)N\varepsilon + Nn_i E(n_i). \quad (3)$$

Using the equilibrium condition $\partial F/\partial y = 0$, we get

$$|\varepsilon| = \frac{(x - 1)^2 Q^2}{2C y^2}. \quad (4)$$

The physical meaning is obvious. If we take one complex out of the macroscopic drop, we lose correlational energy ε but also reduce the Coulomb energy of the system $(x-1)^2 Q^2 / 2C y^2$ since total charge is shared by one more free complex. They are equal at the equilibrium.

For a PA with length L and distances between charges b ($L \gg b$), when $r_s \rightarrow \infty$, we have

$$C = \frac{DL}{2 \ln(L/b)}, \quad (5)$$

where $D = 80$ is the dielectric constant of water. Substituting Eq. (5) into Eq. (4), we get the fraction y as a function of x

$$y(x) = |x-1| \sqrt{\frac{Q^2 \ln(L/b)}{D|\varepsilon|L}}. \quad (6)$$

The condensed drop disappears at $y = 1$. The corresponding values of x are

$$x_{c,d} = 1 \mp \sqrt{\frac{D|\varepsilon|L}{Q^2 \ln(L/b)}}. \quad (7)$$

Here and below the upper (lower) sign corresponds to the first (second) subscript of $x_{c,d}$. We also get the absolute value of the net charge of a free complex in the condensation regime ($x_c < s < x_d$)

$$\frac{|x-1|Q}{y} = \sqrt{\frac{D|\varepsilon|L}{\ln(L/b)}} = (x_d - 1)Q. \quad (8)$$

We see that this value is independent of x [12]. The corresponding phase diagram is shown on the horizontal axis of Fig. 2, if one neglects the tadpole phase.

It should be emphasized that at $x > 1$ side, the state of partial condensation is not always realized. As mentioned in the previous section, at $x > 1$ side, there is another critical value of x , x_{ci} , at which charge inversion of a free complex reaches its maximum value. x_{ci} is determined from the equilibrium condition of a PC,

$$\mu_c = -\frac{(x_{ci} - 1)Qq}{C}, \quad (9)$$

where each free complex carries net charge $(x_{ci} - 1)Q$. Therefore

$$x_{ci} = 1 + \frac{DL|\mu_c|}{2Qq \ln(L/b)}. \quad (10)$$

In the free energy of Eq. (3), we have assumed that all PCs are adsorbed to PAs in the condensation regime. This is true only if $x_d < x_{ci}$ and leads to the phase diagram of Fig. 2.

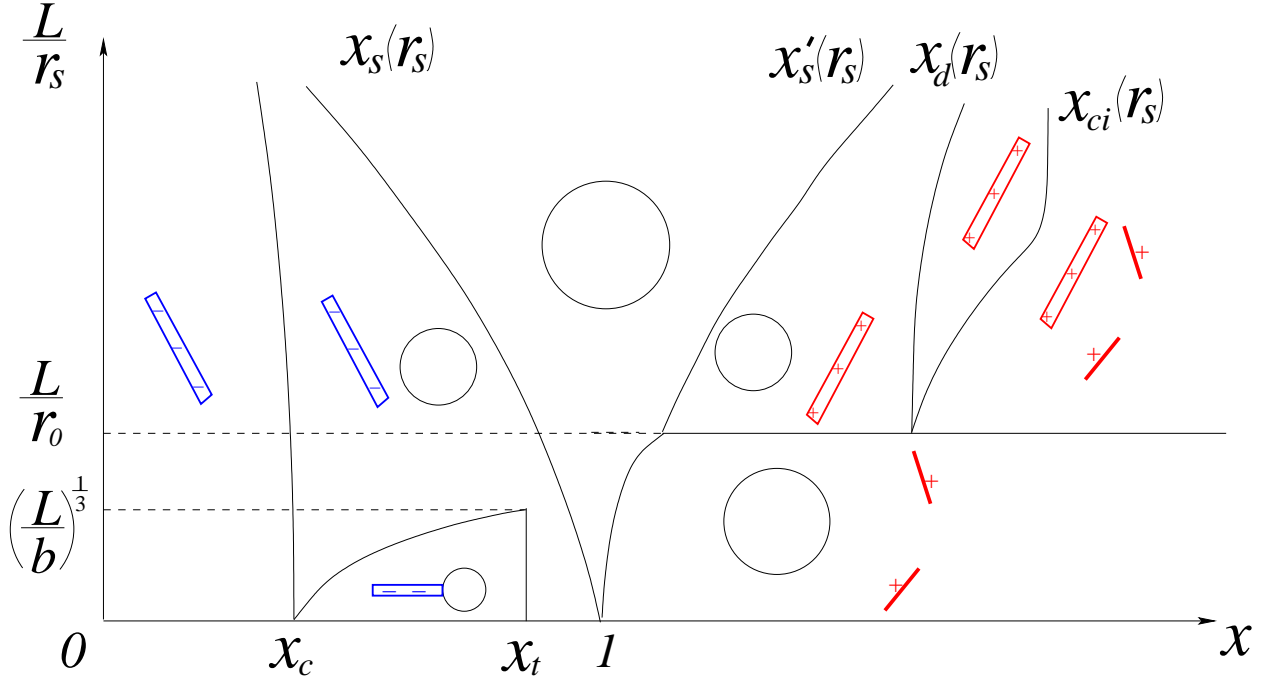


FIG. 6: Phase diagram of solution of PA and PC in the case where at $r_s \rightarrow \infty$, we formally have $x_d > x_{ci}$. The meaning of axes and symbols are the same as Fig. 2.

If $x_d > x_{ci}$, according to Eq. (8), each free complex should carry charge $(x_d - 1)Q$ while it is only allowed to carry $(x_{ci} - 1)Q$ because of the finite correlation chemical potential μ_c . In this case, x_d loses its physical meaning and Eq. (3) should be revised to

$$F(y) = yN \frac{(x_{ci} - 1)^2 Q^2}{2C} + yN \frac{(x_{ci} - 1)Q}{q} \mu_c + (1 - y)N\varepsilon + Nn_i E(n_i), \quad (11)$$

in which the charge of each free complex is saturated at the maximum value, $(x_{ci} - 1)Q$. With help of Eqs. (7) and (9), this free energy can be written as

$$F(y) = -yN \frac{(x_{ci} - 1)^2 Q^2}{2C} - (1 - y)N \frac{(x_d - 1)^2 Q^2}{2C} + Nn_i E(n_i). \quad (12)$$

Clearly, when $x_d > x_{ci}$, the minimum of $F(y)$ is reached at $y = 0$. Therefore at $x > 1$ side, we arrive at a phase of total condensation in which all complexes are condensed (see the horizontal axis of Fig. 6).

In order to clarify the meaning of the condition $x_d = x_{ci}$, we rewrite it as

$$\varepsilon = \frac{(x_{ci} - 1)^2 Q^2}{2C} + \frac{(x_{ci} - 1)Q}{q} \mu_c. \quad (13)$$

For a neutral complex, the left hand side is its correlational energy gain in the macroscopic drop while the right hand side is the reduction of its free energy due to maximum overcharging. If the left hand side is larger in absolute value, or $x_d > x_{ci}$, a neutral condensed complex has lower free energy than a free complex in which charge inversion reaches its maximum value. All of complexes condense.

Interestingly, both two cases of $x_d < x_{ci}$ and $x_d > x_{ci}$ at $r_s \rightarrow \infty$ are realistic as we will see in Sec. V.

III. INTRA-COMPLEX DISPROPORTIONATION

In this section, we discuss intra-complex disproportionation in which PCs disproportionate themselves within each complex so that each complex forms a “tadpole” with a neutral condensed “head” and a charged “tail” (Fig. 5b). We show that “intra” is better than “inter” in a certain range of x (see Fig. 2). Again, in this section, we assume $r_s \rightarrow \infty$ and leave the discussion of the screening effect of monovalent salt to the next section.

Let us first assume that the tadpole configuration shown in Fig. 5b is the best for intra-complex disproportionation. We will verify this assumption at the end of this section. When discussing inter-complex disproportionation, we defined y as the fraction of free complexes in the solution. In the case of intra-complex disproportionation, we use a similar quantity, z , to denote the fraction of the tail part of each complex. The free energy of the system is simply N times of the free energy of each complex. Similarly to Eq. (3),

$$F(z) = N \frac{(x-1)^2 Q^2}{2C_t} + N \frac{(x-1)Q}{q} \mu_c + (1-z)N\varepsilon + Nn_i E(n_i) - N(1-z)\varepsilon \frac{3b}{R}. \quad (14)$$

Here the radius of a head

$$R = \left[\frac{3}{16} (1-z)b^2 L \right]^{1/3} \quad (15)$$

(see Fig. 5b), and

$$C_t = \frac{DzL}{2 \ln(zL/b)} \quad (16)$$

is the capacitance of the tadpole almost totally determined by the length of its tail, zL . In Eq. (14), the meaning of the first four terms is similar to Eq. (3) except that condensed and charged pieces coexist in each complex now. Comparing with Eq. (3), we see that in the first term of the Coulomb energy, instead of $\ln(L/b)$, we have $\ln(zL/b)$ due to the change of the length of the free complex. The last term is new and takes into account of the

surface energy of every head [15]. The change of the logarithm in the capacitance gives a negative correction to the free energy Eq. (3), while the surface energy term gives a positive correction.

To compare the free energy minimum of Eq. (14) with Eq. (3), we first solve $\partial F/\partial z = 0$ ignoring the two small corrections in Eq. (14), which gives

$$z(x) = |x - 1| \sqrt{\frac{Q^2 \ln(L/b)}{D|\varepsilon|L}}. \quad (17)$$

It is the same as Eq. (6) if z is replaced by y . Indeed the main terms in Eq. (3) and Eq. (14) and their minimums are the same. As a result, the boundaries of the condensation regime $x_{c,d}$ are not changed. Then subtracting Eq. (3) with optimal y determined by Eq. (6) from Eq. (14) with optimal z determined by Eq. (17), we can find the total correction to the free energy due to transition from the phase of partial condensation to the tadpole phase

$$\Delta F = -\frac{(x-1)^2 Q^2 \ln(1/z)}{DzL} + (1-z)|\varepsilon| \frac{3b}{R}. \quad (18)$$

Here the first term is the negative correction to the Coulomb energy due to increasing capacitance. The second term is the positive correction due to the surface energy. Using Eq. (17), the critical value of z for $\Delta F = 0$ is

$$z_t \simeq \left(\frac{b}{L}\right)^{1/3}. \quad (19)$$

For $z > z_t$ (t stands for ‘‘tadpole’’), the negative correction to the Coulomb energy dominates, and the tadpole phase is preferred. For $z < z_t$, the positive correction of the surface energy dominates, and the phase of partial condensation is preferred. According to Eq. (17), the corresponding x at two sides of $x = 1$ are

$$x_t \simeq 1 - \left(\frac{b}{L}\right)^{1/3} \sqrt{\frac{D|\varepsilon|L}{Q^2 \ln(L/b)}}. \quad (20)$$

$$x'_t \simeq 1 + \left(\frac{b}{L}\right)^{1/3} \sqrt{\frac{D|\varepsilon|L}{Q^2 \ln(L/b)}}. \quad (21)$$

As shown in Fig. 2, when $r_s \rightarrow \infty$, the tadpole phase dominates at $x_c < x < x_t$ and $x'_t < x < x_d$, while the phase of partial condensation dominates at $x_t < x < x'_t$. In the case of $x_d > x_{ci}$, only x_t is meaningful (see Fig. 6).

In the end of this section, let us argue that the one-head-one-tail tadpole configuration is the best for intra-complex disproportionation. To do this, we have to include the capacitance

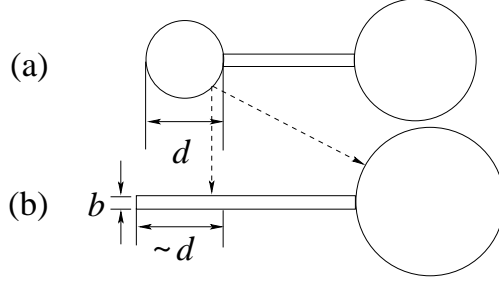


FIG. 7: Comparison of two-heads with one-head. (a): a two-head configuration. The diameter of the smaller head is d . (b): a one-head configuration made from (a) by combining the two heads then releasing tail of length order of d from the head, such that the two configurations have same capacitance. The Coulomb energy is the same for the two configurations, but the surface energy is higher in (a).

of heads which gives a small correction to Eq. (16). First of all, let us show that for a complex with given charge, one head is better than two heads. Consider an arbitrary two-heads configuration with the diameter of the smaller head d (Fig.7a). We can always construct an one-head configuration from it by combining the two heads then releasing additional tail of the order of d from the head in such a way that the capacitances of the two configurations are the same (Fig.7b). The total free energy consists of the long-range Coulomb energy and the short-range correlation energy in droplets. For the two configurations, the Coulomb energies are the same since the capacitances are equal. But the correlation energy is higher in the two-heads configuration since the surface is much larger. Actually, the difference in the surface energy is proportional to $d^2/b - d \simeq d^2/b$. Thus, for any two-heads configuration, we can always find a one-head configuration with lower energy. By similar argument, a configuration of many heads is even worse. Furthermore, the head always prefers to be at the end of the tail. This can be understood by considering a metallic stick with fixed charge on it. The electric field is larger at the end of the stick than in the middle. Therefore to reduce the Coulomb energy, it is better to put a metallic sphere at the end of the stick.

IV. THE EFFECTS OF SCREENING BY MONOVALENT SALT

In this section we discuss the effects of a finite r_s . The r_s range we are interested in is $b < r_s < L$. As r_s becomes smaller than L , the long-range Coulomb repulsion is first

reduced while the short-range correlational attraction is not affected. Eventually, when $r_s < b$, the short-range correlational attraction is also screened out and the macroscopic drop completely dissolves. In the range of $b \ll r_s \ll L$, there are three major implications of screening (see Fig. 2). Firstly, x_{ci} and $x_{c,d}$ are changed and the condensation regime in the phase diagram widens. Secondly, the phase of single drop grows up. Thirdly, the tadpole phase is destroyed. Below we discuss these three implications.

A. The change of x_{ci} and $x_{c,d}$

When $b \ll r_s \ll L$, the capacitance of a free complex is increased to

$$C = \frac{DL}{2 \ln(r_s/b)}. \quad (22)$$

Using Eq. (4), we get

$$x_{c,d}(r_s) = 1 \mp \sqrt{\frac{D|\varepsilon|L}{Q^2 \ln(r_s/b)}}. \quad (23)$$

We see that x_c decreases and x_d increases with decreasing r_s . The condensation regime is enlarged (see Fig. 2).

On the other hand, according to Eq. (9), we have

$$x_{ci}(r_s) = 1 + \frac{DL|\mu_c|}{2Qq \ln(r_s/b)}. \quad (24)$$

Notice that μ_c also depends on r_s .

In the case where $x_d > x_{ci}$ at $r_s \rightarrow \infty$, decreasing r_s eventually leads to inversion of inequality $x_d > x_{ci}$ and phase diagram Fig. 6. We discuss this effect in the next section after we estimate ε and μ_c microscopically.

B. Expansion of the range of the single drop phase

As discussed in Sec. I, when $r_s \rightarrow \infty$, the macroscopic condensate is almost neutral and the phase of single drop exist only at $x = 1$. For finite r_s , the macroscopic drop can tolerate certain charge density. The range of the single drop phase grows with L/r_s as shown in Fig. 2. Quantitatively, the tolerance of charge in the macroscopic drop can be described by the capacitance of a condensed complex, C' . In order to calculate C' , we assume that the macroscopic drop is uniformly charged [16]. If the charge density of the macroscopic drop is

ρ and the charge of each complex is $\pi b^2 L \rho / 4$ [15], the electrical potential of the macroscopic drop is

$$\phi = \int_0^\infty \frac{\rho e^{-r'/r_s}}{Dr'} 4\pi r'^2 dr' = \frac{4\pi r_s^2 \rho}{D}, \quad (25)$$

This gives

$$C' = \frac{\pi b^2 L \rho}{4\phi} = \frac{Db^2 L}{16r_s^2}. \quad (26)$$

When $r_s \rightarrow \infty$, the capacitance $C' \rightarrow 0$ as expected.

In the case of $x_d < x_{ci}$ at $r_s \rightarrow \infty$, taking into account of C' , similarly to Eq. (3), we have

$$F(y) = \frac{N^2(x-1)^2 Q^2}{2[yNC + (1-y)NC']} + \frac{N(x-1)Q}{q} \mu_c + (1-y)N\varepsilon + Nn_i E(n_i). \quad (27)$$

Here the first term is the Coulomb energy of the system of free and condensed complexes with capacitances C and C' correspondingly. These capacitances are additive because all complexes are in equilibrium with respect of exchange of PC and the electric potential of all complexes is the same.

With help of Eqs. (22) and (26), the equilibrium condition $\partial F / \partial y = 0$ reads

$$(x-1)^2 \left[\frac{1}{\ln(r_s/b)} - \frac{b^2}{8r_s^2} \right] = \frac{D|\varepsilon|L}{Q^2} \left[\frac{y}{\ln(r_s/b)} + \frac{(1-y)b^2}{8r_s^2} \right]^2 \quad (28)$$

Putting $y = 0$, we get boundaries of the single drop phase

$$x_s(r_s) = 1 - \frac{b^2}{8r_s^2} \sqrt{\frac{D|\varepsilon|L \ln(r_s/b)}{Q^2}} \quad (29)$$

$$x'_s(r_s) = 1 + \frac{b^2}{8r_s^2} \sqrt{\frac{D|\varepsilon|L \ln(r_s/b)}{Q^2}}. \quad (30)$$

As shown in Fig. 2, in the range of $x_s(r_s) < x < x'_s(r_s)$ (s stand for ‘‘single drop’’), there is no free complexes or free PC, only a single drop. The width of the single drop phase grows proportionally to $1/r_s^2$ with decreasing r_s . When $r_s \rightarrow \infty$, both $x_s(r_s), x'_s(r_s) \rightarrow 1$ as expected.

In the case where $x_d > x_{ci}$ at $r_s \rightarrow \infty$, the phase of single drop again expands around $x = 1$ with growing L/r_s (see Fig. 6). At $x < 1$ side, x_s is still given by Eq. (29). At $x > 1$ side, there is a critical value $r_s = r_0$ where inequality $x_d(r_s) > x_{ci}(r_s)$ is inverted (see the next section for calculation of r_0). At $r_s > r_0$, we have the phase of total condensation, where all complexes are condensed in a macroscopic drop but excessive PCs are free. What

we need to find out is just how many excessive PCs the macroscopic drop can tolerate at finite r_s . Applying the condition of maximum charge inversion to a condensed complex,

$$\mu_c = -\frac{(x'_s - 1)Qq}{C'}, \quad (31)$$

we get

$$x'_s(r_s) = 1 + \frac{D|\mu_c|b^2L}{16Qqr_s^2}. \quad (32)$$

Again, when $r_s \rightarrow \infty$, $x'_s(r_s) \rightarrow 1$. One can check that $x'_s(r_s)$ given by Eq. (32) is larger than $x'_s(r_s)$ given by Eq. (30), when $x_d(r_s) > x_{ci}(r_s)$. At $r_s < r_0$, we arrive at inequality $x_d(r_s) < x_{ci}(r_s)$ and Eq. (30) gives the boundary of the phase of single drop (see Fig. 6). We will discuss the transition at $r_s = r_0$ in detail in the next section.

C. Extinction of tadpoles

Let us discuss how finite r_s affects competition between inter-complex disproportionation, or the phase of partial condensation, and intra-complex disproportionation, or the tadpole phase (see Fig. 5). The tadpole phase is better in the Coulomb energy since charges are distributed among all complexes, but worse in the surface energy since each complex has a condensed droplet. When $b \ll r_s \ll L$, the Coulomb energy is reduced while the surface energy which originates from the short-range correlation is not affected. Therefore the range of the tadpole phase in the phase diagram shrinks (see Fig. 2). At certain critical r_s , it loses to the phase of partial condensation everywhere. For simplicity, in this subsection we only discuss $x < 1$ side. Similar results can be got at $x > 1$ side in the case where $x_d < x_{ci}$ (see Fig. 2).

In order to discuss the additional capacitance of the tadpole phase, it is necessary to consider two separate cases: $zL \ll r_s \ll L$ and $b \ll r_s \ll zL$. Let us start from $zL \ll r_s \ll L$. In this case, the capacitance of each tadpole is determined by its tail and still given by Eq. (16). According to it, the free energy of Eq. (14) can be written as [15]

$$F(z) = N \frac{(x-1)^2 Q^2}{DzL} \ln(r_s/b) + (1-z)N\varepsilon + N \frac{(x-1)Q}{q} \mu_c + Nn_i E(n_i) + \left[-N \frac{(x-1)^2 Q^2}{DzL} \ln(r_s/zL) - N(1-z)\varepsilon \frac{3b}{R} \right]. \quad (33)$$

In the expression, the last two terms in the square bracket are the corrections to the first two terms. The first one is the negative correction to the Coulomb energy due to increasing

capacitance, while the second one is the positive correction due to the surface energy of all heads. Without these two corrections, the free energy of the tadpole phase is the same as that of the phase of partial condensation given by Eq. (3) and Eq. (22), if y is replaced by z . Similarly to what we did in the last section, we first solve $\partial F/\partial z = 0$ without the two corrections to get

$$z(x) = |x - 1| \sqrt{\frac{Q^2 \ln(r_s/b)}{D|\varepsilon|L}}, \quad (34)$$

which is also the equilibrium condition for Eq. (3) if z is replaced by y . Then letting the two corrections equal to zero

$$\frac{(x-1)^2 Q^2}{DzL} \ln(r_s/zL) + (1-z)\varepsilon \frac{3b}{R} = 0, \quad (35)$$

and substituting Eq. (34) into it, we get critical values of z and x as a function of r_s

$$z_1(r_s) \simeq \left(\frac{b}{L}\right)^{1/3} \quad (36)$$

$$x_1(r_s) \simeq 1 - \left(\frac{b}{L}\right)^{1/3} \sqrt{\frac{D|\varepsilon|L}{Q^2 \ln(r_s/b)}}. \quad (37)$$

When $x < x_1$, the tadpole phase wins. While when $x > x_1$, the phase of partial condensation wins.

The case of smaller r_s , where $b \ll r_s \ll zL$ is a little more complicated. In this case, the capacitance of a tadpole determined by its tail is given by

$$C_t = \frac{DzL}{2 \ln(r_s/b)}. \quad (38)$$

It seems that if $y = z$, the total capacitance of the tadpole phase which is N times of Eq. (38) is equal to the total capacitance of the phase of partial condensation which is yN times of Eq. (22). But this is not true since we have ignored the additional capacitance of the two edges of each free complex in deriving Eqs. (22) and (38). It is well known that for a charged metallic cylinder with finite length, the linear charge density at the edges of the cylinder is larger. Therefore the edges contribute more to the capacitance. In the tadpole phase, since all complexes are free, there are more edges. Hence the capacitance is larger and Coulomb energy is smaller.

The edge capacitance can be estimated as follows. As we know, the total capacitance of two cylinders with length L and radius r is $L/\ln(L/b)$. While the capacitance of one

cylinder with length $2L$ is $L/\ln(2L/b)$. Since the cylinder of $2L$ is just combination of two cylinders of L without two edges, the two edges contribute the capacitance

$$C_{edge} = \left(\frac{L}{\ln(L/b)} - \frac{L}{\ln(2L/b)} \right) = \frac{L \ln 2}{\ln(L/b) \ln(2L/b)} \simeq \frac{L \ln 2}{\ln^2(L/b)}. \quad (39)$$

In the case where $r_s \ll L$, a cylinder with length L can be considered as combination of many cylinders with length r_s . Therefore the capacitance of the two edges is

$$C_{edge} \simeq \frac{r_s \ln 2}{\ln^2(r_s/b)}. \quad (40)$$

If this edge capacitance is included, the total capacitance of the tadpole phase is larger. Note that for a tadpole, the capacitance of the head is negligible when $r_s \gg R$. We show later that this is always true when the tadpole phase exists.

Now we compare the free energies of the two phases given by Eqs. (3) and (14). For mathematical convenience, we replace y by z in Eq. (3). Similarly to what we did to Eq. (33), we solve $\partial F/\partial z = 0$ for the main terms in the two free energies without the edge capacitance and the surface energy terms to get Eq. (34). We then set the correction terms to the two phases equal

$$-\frac{(x-1)^2 Q^2 r_s \ln 2}{DzL^2} + (1-z)\varepsilon \frac{3b}{R} = -\frac{(x-1)^2 Q^2 r_s \ln 2}{Dz^2 L^2}. \quad (41)$$

The left hand side is the correction terms in the tadpole phase related to the edge capacitance and the surface energy of heads. The right hand side is the correction term in the phase of partial condensation related to the edge capacitance. Using Eq. (34), we get another critical values of z and x as a function of r_s

$$z_2(r_s) \simeq 1 - \frac{b}{L} \left(\frac{L}{r_s} \right)^3 \ln^3(r_s/b) \quad (42)$$

$$x_2(r_s) \simeq 1 - \left[1 - \frac{b}{L} \left(\frac{L}{r_s} \right)^3 \ln^3(r_s/b) \right] \sqrt{\frac{D|\varepsilon|L}{Q^2 \ln(r_s/b)}}. \quad (43)$$

When $x < x_2$, the phase of partial condensation is preferred. When $x > x_2$, the tadpole phase is preferred.

Combining both cases discussed above, we arrive to the picture shown in Fig. 2. The tadpole phase is preferred for $x_2 < x < x_1$, while the phase of partial condensation is preferred for $x_c < x < x_2$ and $x_1 < x < 1$. At $r_s = L$, $x_2 \rightarrow x_c$ and $x_1 \rightarrow x_t$. As r_s decreases, x_2 increases and x_1 decreases (In the phase diagram, we do not show the

dependence of x_1 on r_s since it is only logarithmical which is much weaker than dependence of x_2 on r_s). Finally, at $r_s \simeq b^{1/3}L^{2/3}$, x_2 merges with x_1 . For smaller r_s , the tadpole phase vanishes. We see that the tadpole phase exists only at $r_s \gg R \simeq b^{2/3}L^{1/3}$ which verifies that the capacitance of the head can be neglected. Also, as expected, for $r_s \gg b^{1/3}L^{2/3}$, $z_1L \ll r_s$ and $z_2L \gg r_s$ for $x = x_1(r_s)$ and $x = x_2(r_s)$ correspondingly.

V. PHASE DIAGRAM OF STRONGLY CHARGED POLYELECTROLYTES

In this section, we consider a simple system where linear charge densities of PA's and PC's are equal. Both of them are strongly charged such that every monomer carries a fundamental charge e and $e^2/Db \simeq k_B T$ (see Fig. 3). We estimate parameters ε and μ_c microscopically and choose from the two phase diagrams shown in Figs. 2 and 6.

We first consider the case of $r_s \rightarrow \infty$. As discussed in Sec. I, μ_c is equal to the Coulomb self-energy of a PC,

$$\mu_c = -\frac{qe}{Db} \ln(q/e). \quad (44)$$

On the other hand, when neutral PA-PCs complexes condense, they form a strongly correlated liquid. Monomers of two PEs locally form NaCl-like structure such that the energy in order of $-e^2/Db$ per monomer is gained (Fig. 4) [15]. Therefore

$$\varepsilon \simeq -\frac{Qe}{Db}. \quad (45)$$

Substituting $L = Qb/e$ into Eqs. (7) and (10), we have

$$x_{c,d} \simeq 1 \mp \frac{1}{\sqrt{\ln(Q/e)}}, \quad (46)$$

$$x_{ci} = 1 + \frac{\ln(q/e)}{2 \ln(Q/e)}. \quad (47)$$

Accordingly, we get the critical value of q at which $x_d = x_{ci}$,

$$q_c = \exp\left(2\sqrt{\ln(Q/e)}\right), \quad (48)$$

where c stands for ‘‘critical’’. When $q > q_c$, or PC is long enough, $x_d < x_{ci}$, we have the phase diagram of reentrant condensation (horizontal axis of Fig. 2). When $q < q_c$, or PC is relatively short, $x_d > x_{ci}$, we have the asymmetric phase diagram with total condensation at $x > 1$ side (horizontal axis of Fig. 6). The possibility of having two different phase diagrams

for different q is related to the interplay of the logarithms in Eqs. (44) and (47). For fixed Q , when q increases, x_{ci} increases but x_d is fixed. Therefore we can have either $x_{ci} < x_d$ or $x_{ci} > x_d$ by changing q . Notice that q_c is exponentially smaller than Q .

Now let us consider the effect of screening by monovalent salt. We are interested in the case of $r_s \gg b$ where the short-range correlation is not affected yet and ε is fixed. According to Eq. (23),

$$x_{c,d}(r_s) \simeq 1 \mp \frac{1}{\sqrt{\ln(r_s/b)}}, \quad (49)$$

When $qb/e \ll r_s \ll Qb/e$, the chemical potential μ_c is still given by Eq. (44). From Eq. (24),

$$x_{ci}(r_s) = 1 + \frac{\ln(q/e)}{2 \ln(r_s/b)}. \quad (50)$$

Accordingly, the critical value of q at which $x_d(r_s) = x_{ci}(r_s)$ is

$$q_c(r_s) = \exp \left[2\sqrt{\ln(r_s/b)} \right]. \quad (51)$$

It decreases with decreasing r_s . Therefore, for a system with $q < q_c$, q can be larger than $q_c(r_s)$ at small r_s . Correspondingly, at $x > 1$, for small r_s , the phase of total condensation is replaced by the phase of partial condensation. We have a phase diagram shown in Fig. 6. Letting $q = q_c(r_s)$, we get the critical value of r_s at which this phase transition happens

$$r_0 = b \exp \left(\frac{\ln^2(q/e)}{4} \right). \quad (52)$$

Notice that r_0 is much larger than qb/e .

In Fig. 6, $x_d(r_s) > x_{ci}(r_s)$ at $r_s > r_0$, while $x_d(r_s) < x_{ci}(r_s)$ at $r_s < r_0$ (curves not shown). By definition of r_0 , the curves $x_d(r_s)$ and $x_{ci}(r_s)$ merge at $r_s = r_0$. The curve $x'_s(r_s)$ is given by Eq. (32) for $r_s > r_0$ and Eq. (30) for $r_s < r_0$. At $r_s = r_0$, these two expressions are equal to each other. At $x > 1$ side, the solid line at $L/r_s = L/r_0$ corresponds to a first order phase transition. Notice that L/r_0 can be either larger or smaller than $(L/b)^{1/3}$. Here for simplicity, only the former case is shown in Fig. 6.

When $b \ll r_s \ll qb/e$,

$$\mu_c = -\frac{qe}{Db} \ln(r_s/b), \quad (53)$$

and $x_{ci}(r_s) = 3/2$ [14]. In this case, we always have $x_d(r_s) < x_{ci}(r_s)$ as shown in Figs. 2 and 6.

Finally, in all cases discussed above, the values of $x_{c,d}$ are close to 1, i.e., $|n - n_i| \ll n_i$ in the condensation regime. Therefore the approximation used in Sec. II that μ_c is a constant is valid.

VI. THE ROLE OF THE TRANSLATIONAL ENTROPY

A major approximation in this paper is that the translational entropy of PCs is negligible (we can always ignore PA's translational entropy since it is much longer than PC). In this section, we would like to discuss the validity of this approximation and the role of the translational entropy.

First, let us estimate when this approximation is valid. Consider PCs with concentration p in the solution. The free energy due to its translational entropy is $k_B T \ln(pv_0)$, where v_0 is the normalizing volume. On the other hand, according to Eq. (44), the Coulomb energy is in the order of $-qe/Db \simeq -qk_B T/e$. Letting them equal to each other, we get a critical value, $p = \exp(-q/e)/v_0$. Therefore for a long PC with large q , we can ignore PC's translational entropy even at exponentially small p .

If PC is very short, its translational entropy should be included. DNA with short polyamines is a good example [9, 10, 11]. In this case, the phase diagram gets another dimension, say, the concentration of PC, p . This effect was discussed in detail in Ref. [12, 13] in which the phase diagram is drawn in a plane of two concentrations of oppositely charged colloids. Here in the connection with them, we discuss the same effect in the language of total charge ratio x used in this paper in the simple case where $x_d > x_{ci}$ and $r_s \rightarrow \infty$. For simplicity, we neglect the possibility of intra-molecule disproportionation and the tadpole phase.

In the present case, the free energy in Eq. (1) gets an additional term due to the translational entropy of PCs [12]

$$\begin{aligned}
 F(n, y) = & yN \left[\frac{(nq - Q)^2}{2C} + nE(n) \right] + (1 - y)N[n_i E(n_i) + \varepsilon] \\
 & + \left[\frac{NxQ}{q} - yNn - (1 - y)Nn_i \right] \ln \left[\left(p - \frac{ynq}{xQ}p - \frac{1 - y}{x}p \right) \frac{v_0}{e} \right], \quad (54)
 \end{aligned}$$

where e is the natural exponential. Here the expression in the square bracket before the logarithm represents the number of free PC in the solution, and the expression in the round bracket in the logarithm represents the corresponding concentration.

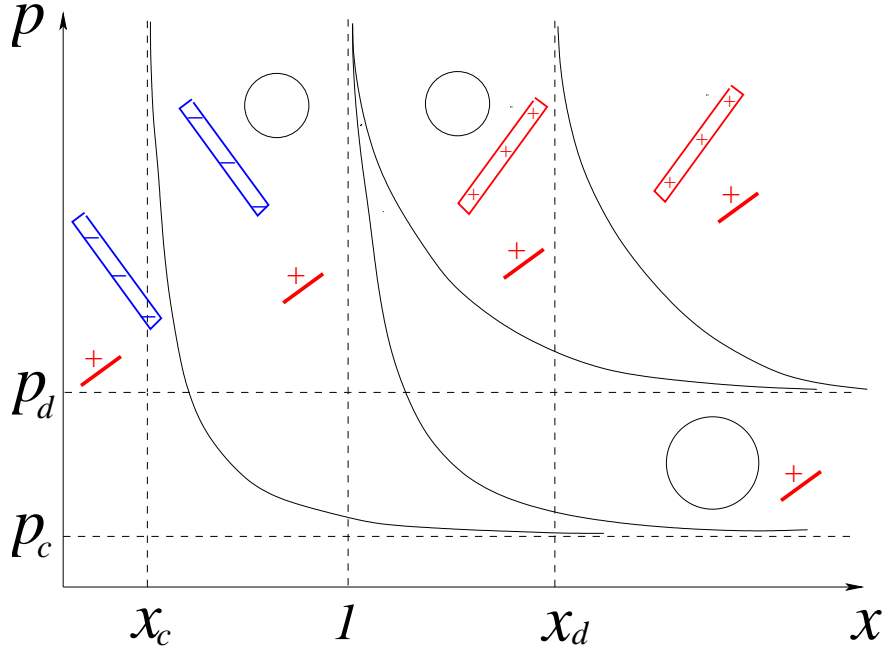


FIG. 8: Phase diagram in a plane of PC's concentration p and total charge ratio x ($x_d > x_{ci}$ and $r_s \rightarrow \infty$). Symbols used are explained in Fig. 1. It shows how the phase of total condensation replaces that of partial condensation with decreasing p .

Now n and y are two independent variables. Taking $\partial F/\partial n = 0$ and $\partial F/\partial y = 0$, we get

$$\mu_c = \ln \left[\left(p - \frac{ynq}{xQ}p - \frac{1-y}{x}p \right) v_0 \right] - \frac{(nq - Q)q}{C}, \quad (55)$$

$$\varepsilon = \frac{(nq - Q)^2}{2C} + (n - n_i) \left\{ \mu_c - \ln \left[\left(p - \frac{ynq}{xQ}p - \frac{1-y}{x}p \right) v_0 \right] \right\}. \quad (56)$$

In Eq. (55), eliminating n by Eq. (56), we can calculate the boundaries of the condensation regime by setting $y = 0$ and $y = 1$. For $y = 0$, we get two boundaries of a total condensation regime,

$$p \left(1 - \frac{1}{x} \right) = p_{c,d}. \quad (57)$$

For $y = 1$, we get two boundaries between the partial condensation regime and the free complexes regime,

$$p \left(1 - \frac{x_{c,d}}{x} \right) = p_{c,d}. \quad (58)$$

Here

$$p_{c,d} = \frac{1}{v_0} \exp \left(\mu_c \mp \sqrt{\frac{2|\varepsilon|q^2}{C}} \right). \quad (59)$$

Accordingly, as shown in the phase diagram Fig. 8, a regime of total condensation is sandwiched by two regimes of partial condensation, which are further sandwiched by two regimes of free complexes.

In Fig. 8, results of previous sections corresponds to the limiting value of $p \rightarrow \infty$. With the translational entropy of PC, or finite p , all critical x are shifted to higher values. At the same time, a total condensation region appears even in the absence of monovalent salt [12]. In the limiting case where $x \rightarrow \infty$, the concentration of PA is much smaller than that of PC, and the entropy of PC is fixed which offers a fixed charging voltage to PA. As a result, all PA-PCs complexes are either totally condensed or totally free. The partial condensation regime disappears [12].

VII. CONCLUSION

In this paper, we discussed complexation and condensation of PA with PC in a salty water solution. Using ideas of disproportionation of PCs among complexes and inside complexes (inter- and intra-complex disproportionations) we arrived at the two phase diagrams in a plane of x and L/r_s shown in Figs. 2 and 6. The phase diagram in Fig. 2 is valid when in the limit $r_s \rightarrow \infty$, $x_d < x_{ci}$. The phase diagram in Fig. 6 works in the opposite case. In the case of strongly charged PA and PC, we find that both two phase diagrams are possible depending on the relative length of PC to PA. Fig. 2 corresponds to more generic case of relatively long PC, while Fig. 6 to the case of relatively short one. Our phase diagrams show how total condensation is replaced by the partial one and then by phases of stable complexes when x moves away from $x = 1$.

We discovered the main two new features of the diagrams. First, at large screening radius they include a new phase of tadpoles. Second, we found that the phase of the single drop formed at x close to 1 widens with decreasing r_s as $1/r_s^2$.

Although we talked about strongly charged PA and PC one can also consider phase diagram of weakly charged PA and PC and develop a microscopic theory for it. In both cases, the qualitative picture is the same since our discussion of the phase diagram is rather general and independent of the microscopic mechanism of the short-range attraction.

As mentioned in the introduction, the problem we solved in this paper should be considered as a part of a very general problem of the phase diagram of the solution of two oppositely

charged colloids. An important system of this kind is a long PA with many strongly charged positive spheres. When long double helix DNA plays the role of PA, this system is a model for the natural chromatin. Therefore, we call such system artificial chromatin [12]. Our phase diagrams with all new features should be valid for artificial chromatin as well.

There is another class of systems where only some of our predictions are applicable. In the Ref. [13] we considered solution of large negative spheres with smaller positive ones. Complexation and condensation of such spheres obey the phase diagrams similar to discussed above. For example, screening by monovalent salt again leads to $1/r_s^2$ expansion of the range of the single drop (total condensation) phase. Another our prediction, the tadpole phase, however, is not applicable to this case, because it is essentially based on the polymer nature of PA.

In the case that the role of PA is played by DNA, one should remember that the double helix DNA is so strongly charged that the effect of the Manning condensation by monovalent counterions must be included [12]. Since DNA is complexing with positive objects (PC, positive spheres or multivalent cations), this Manning condensation can be incomplete comparing with free DNA and the effect of counterion release can be important. The quantitative description of this effect depends on the geometry of the positive objects and the microscopic structure of the complex in the system [12]. Generally speaking, this effect leads to the renormalization of charge of PA, Q , used for example for calculation of x . In this case, total condensation still happens around $x = 1$. This means that if on the other hand x is evaluated using the bare charge of DNA, all phase diagrams are centered around a smaller than 1 value of x .

Our phase diagrams deal with equilibrium states of the system. But not all of them can be achieved in experimental time scale due to slow kinetics. Therefore it is not easy to directly compare our theory to experiments. For instance, a phase of many condensed particles with finite size is often found in experiments which does not appear in our phase diagram [1, 2, 3, 7]. We believe that this phase is not a real equilibrium state, but the state frozen kinetically [17]. Thus, kinetics is extremely important for applications and we plan to address it in the future.

Acknowledgments

The authors are grateful to V. Budker, A. Yu. Grosberg, and M. Rubinstein for useful discussions. This work was supported by NSF No. DMR-9985785 and DMI-0210844.

-
- [1] V. Budker, V. Trubetskoy, J. A. Wolff, Condensation of non-stoichiometric DNA/Polycation complexes by divalent cations.
 - [2] A.V. Kabanov and V. A. Kabanov, Bioconjugate Chem. 6 (1995) 7. And references therein.
 - [3] E Lai and J. H. van Zanten, Biophys. J. 80 (2001) 864.
 - [4] K. Minagawa, Y. Matsuzawa, K. Yoshikawa, M. Matsumoto, M. Doi, FEBS Letts. 295 (1991) 67.
 - [5] D. D. Dunlap, A. Maggi, M. R. Soria, L. Monaco, Nucleic Acids Research 25 (1997) 3095.
 - [6] A. A. Zinchenko, V. G. Sergeyeve, S. Murata, K. Yoshikawa, J. Am. Chem. Soc. 125 (2003) 4414.
 - [7] V. A. Bloomfield, Biopolymers 44, (1997) 269.
 - [8] V. Y. Borue and I. Y. Erukhimovich, Macromolecules 23 (1990) 3625. M. Castelnovo and J.-F. Joanny, Eur. Phys. J. E 6 (2001) 377.
 - [9] M. Olvera de la Cruz, L. Belloni, M. Delsanti, J. P. Dalbiez, O. Spalla and M. Drifford, J. Chem. Phys. 103 (1995) 5781.
 - [10] E. Raspaud, M. Olvera de la Cruz, J. -L. Sikorav, and F. Livolant, Biophys. J. 74 (1998) 381.
 - [11] T. T. Nguyen, I. Rouzina, and B. I. Shklovskii, J. Chem. Phys. 112 (2000) 2562.
 - [12] T. T. Nguyen and B. I. Shklovskii, J. Chem. Phys. 115 (2001) 7298.
 - [13] R. Zhang and B. I. Shklovskii, Phys. Rev. E 69 (2004) 021909.
 - [14] T. T. Nguyen and B. I. Shklovskii, Phys. Rev. Lett. 89 (2002) 018101.
 - [15] In this paper, for simplicity, we do not discriminate between the size of the monomer and the distance between charges in the polymer. This is a reasonable approximation for strongly charged polyelectrolytes ($b \simeq l_B = 7\text{\AA}$).
 - [16] R. Zhang and B. I. Shklovskii, cond-mat/0310321.
 - [17] T. T. Nguyen and B. I. Shklovskii, Phys. Rev. E 65 (2002) 031409. B.-Y. Ha, and A. J. Liu, Europhys. Lett. 46 (1999) 624.